Study on the bowing of monocrystalline silicon MWT+PERC solar cells with different laser-ablation condition

RUOYING PENG[a], XI XI[a,b,*], JIANBO SHAO[a], GUILIN LIU[a], SHAOMIN LI[a], ZHONGLIN LU[c], JIANHUA XU[c], ZHI HUANG[c], XIANGYANG ZHANG[a]
[a]*School of Science, Jiangnan University, Wuxi 214122, China*
[b]*Wuxi Suntech Power Co., Ltd., Wuxi 214028, China*
[c]*Wuxi Sunport Power Technology Co., Ltd., Wuxi 214028, China*

The thinner silicon wafers result in the more serious cells bowing, which increases the fragmentation rate and decrease the conversion efficiency. Based on the laser-ablation process on Metal Wrap Through + Passivated Emitter and Rear Contact (MWT+PERC) solar cells, we studied the effect of the aluminum-silicon (Al-Si) contact area on the bowing by theoretical calculation and Abaqus finite element analysis (FEA). Meanwhile, we proposed a novel rear Al-Si contact pattern of silicon cells to improve the bowing after treatments. The results indicated that the bowing can be improved by adopting the rear surface dotted pattern based on fixed laser-ablation area.

(Received December 7, 2020; accepted August 16, 2021)

Keywords: Aluminum-silicon contact, Laser-ablation, Bowing, MWT+PERC, Solar cells

1. Introduction

The blossom of crystal silicon (c-Si) solar cells in photovoltaic (PV) market significantly motives its cost reduction to enhance its competitiveness [1-4]. Though thinner silicon wafers decrease the fabrication cost, following difficulties in the bowing of solar cells increase unnecessary production cost and mainly reduce module power output [5, 6]. The bowing induced fragmentation is mainly occurred in the subsequent testing, packaging and module production process, which have attracted tremendous attentions [3, 7-9]. The main reason of bowing of solar cells is that the different thermal coefficient expansion (TCE) of aluminum-silicon (Al-Si) material [10-13], where the TCE of Aluminum (Al) is at least one order magnitude larger than that of Si material [14]. The TCE of Al is $2.31\times10^{-5}\,K^{-1}$, while it is only $3.36\times10^{-6}\,K^{-1}$ for Si. With the decrease of temperature after the process of firing and metallization, the shrinkage of Al is faster than that of Si. The surface obvious suffers a compressive stress from the squeeze of Al. When the wafers are sintered at a high temperature, the Al-Si alloy is maintained in liquid phase, accelerating the diffusion of Al and Si atoms in the Al-Si alloy [15]. When the liquid phase of Al-Si is cooled down to solid state, the stress at interfaces is released to form the bowing phenomenon.

Meanwhile, the tendency of thinner Si-wafer has become the mainstream in PV industry [16-17]. The bowing phenomenon has become more significant with the thinner Si-wafer. Hence, the problem has become an important issue which strongly blocks the further development of thin c-Si solar cell and has attracted a lot of researches [18-20]. On the other hand, Metal Wrap Through+ Passivated Emitter and Rear Contact (MWT +PERC) is a novel type of high efficiency thin Si solar cells [21-24] with the application of thinner Si-wafer. The thickness of MWT+PERC has been dropped below 170μm with an excellent performance up to 23% in mass production. However, thinner thickness bring problem of bowing. Since the emitter contact electrode and the base contact electrode are both located on the rear surface, the bowing of MWT+PERC solar cells cannot be adjusted by the front bus-bar electrodes. As a result, the adjustment of rear surface of MWT+PERC cells is a solution to fix the bowing problem. Generally, bowing is affected by the Al-Si contact and the size of contact area has a direct effect on the bowing of c-Si solar cells. To modify the bowing effect, we discussed the bowing of the solar cells from the point of rear laser-ablation in this paper. The influence of different Al-Si contact area on bowing was investigated, which has proposed a novel Al-Si contact pattern on the rear surface to improve the bowing after firing and metallization.

2. Experiments

In this paper, the commercial grade crystalline silicon was applied to fabricate MWT+PERC solar cells. The resistivity of p-type mono-Si wafers used in the experiments was maintained at 0.5~1.5 Ω•cm with thickness around 165±5 μm, and the size of wafer was 158.75 mm×158.75 mm. The experimental flow chart of mono-Si MWT+PERC solar cells was shown in Fig. 1(a), and the structure was shown in Fig. 1(b). The Si wafers were initially perforated by the laser to form 6×6 holes, then they were textured with KOH solution with additives, and cleaned in HCl/HF solution. The low pressure diffusion of $POCl_3$ was followed to form the PN junction. The square resistance was controlled at 97±5 Ohm/sq. after diffusion. Then, the phosphorus-silicon glass (PSG) was removed by etching and form a polished rear surface. After the etching process, the wafers were the reacted with oxygen to generate a thin SiO_2 film on top of the Si wafers. Then, an AlO_X/SiN_X dielectric layer was deposited on the rear surface of the wafers by Plasma Enhanced Chemical Vapor Deposition (PECVD), and a SiN_X:H passivation layer was deposited on the front side. Before screen-printed (SP), a certain pulse laser (532 nm) was used to partially remove the passivation layer covered on the rear surface. During the SP process, the front finger grids and the hole blocking conductive electrode were printed with Ag paste, and the photon generated current was collected by the front finger grids, and was transported to the rear surface by the hole blocking conductive electrode. The electrodes leaded from the front surface to the back by the hole blocking conductive electrode were the cathodes. And the anodes were also on the rear surface, as shown in Fig. 1(b). The rear surface was printed with Al paste to form anodes and a local rear electric field. Al and Si were isolated by AlO_X/SiNx layer in the most of the area. The local Al/Si contact and local rear surface field (LBSF) was limited in specified locations which were irradiated by laser. The rear laser-ablation pattern used in the experiments was a combination of dots and lines, and the rear pattern remained unchanged in the experiments [25].

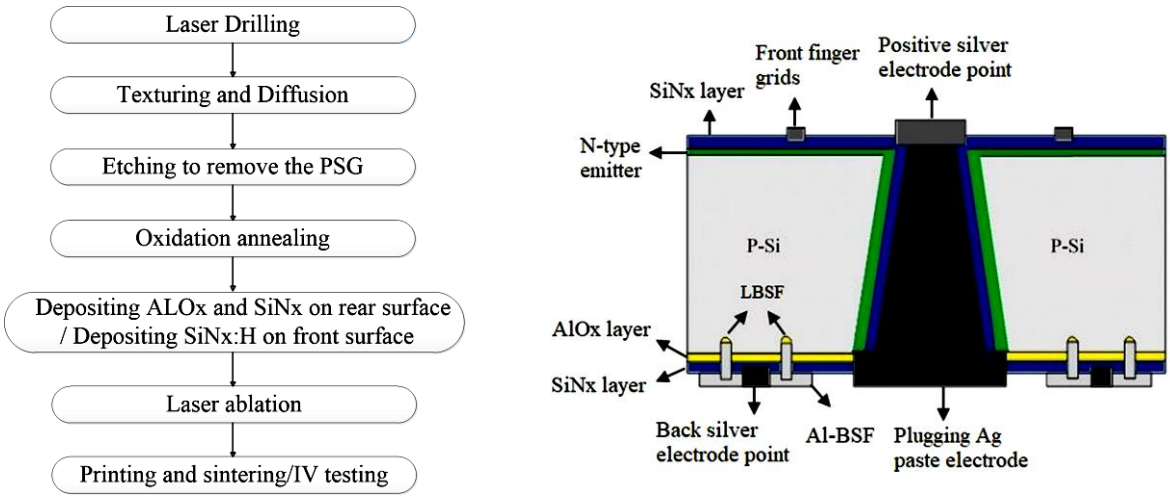

(a) (b)

Fig. 1. (a) Experimental flowchart, (b) The structure of MWT+PERC solar cells (color online)

The bowing effect of cells was defined as the distance δ between the center of the cell and the bottom plane determined by edges of cells, as shown in Fig. 2. The bowing was measured by a feeler gauge in the experiments (three-coordinates measuring machine can also be used) [26].

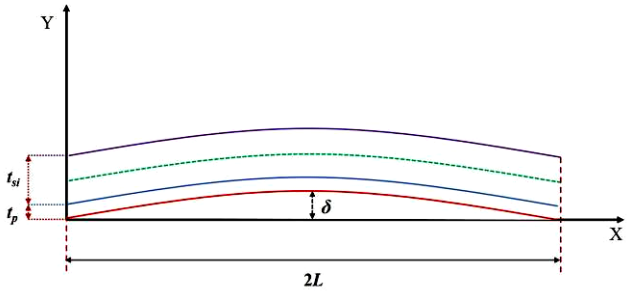

Fig. 2. The model of cell bowing (color online)

3. Results and discussion

The bowing effect can be induced by the different TCE between the front Ag electrodes and Si wafer. Therefore, it is suspected that the front finger grids have certain influences on the bowing effect. Meanwhile, some saw marks will be formed through the Si wafer cutting process. The saw marks and the cross-sectional view were shown in Fig. 3 via the 3D microscope. From the Fig. 3, saw marks were appeared on the surface of the wafers with certain depth after the laser-ablation. Hence, in different laser-ablation direction, the light spot intersects with the line mark is different, which may also have impact on the experimental results. To eliminate the influence of the front finger grids and the direction of laser-ablation on the bowing effect, we have carried out experiments on each aspect separately. In this paper, the same batch mono-Si wafers were divided into two groups with 8 wafers in each. The rear laser-ablation was maintained constant during laser process conditions as well as the contact area (i.e. the laser-ablation ratio). The front finger grids were printed in one set of experiments, and the front electrodes were absent for another set. The two groups were transferred into the same firing conditions to measure the bowing effect. In the same way, in another set of experiments, the laser-ablation direction of one group were parallel to the saw marks direction, the other group was perpendicular to the trace direction. The results of the two groups are shown in Table 1.

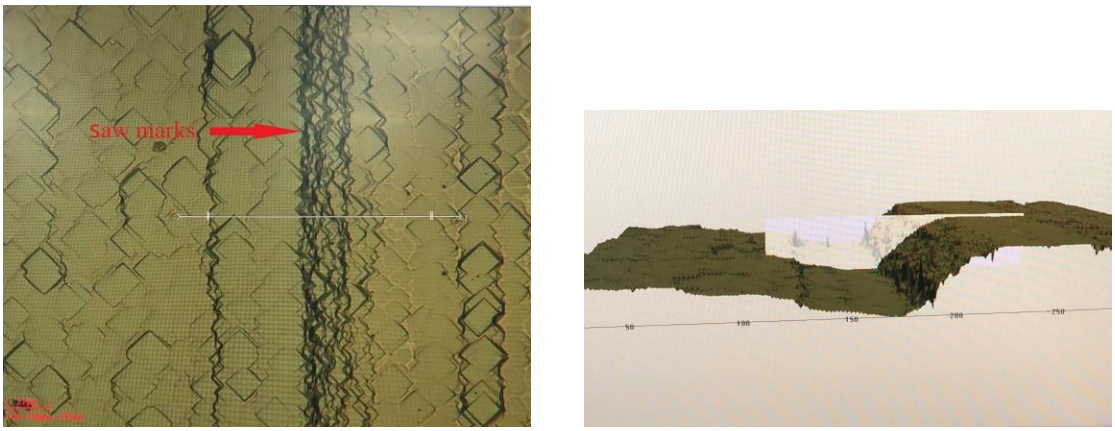

(a) (b)

Fig. 3. Saw marks of silicon wafers under 3D microscope, (a) Saw marks under 3D microscope, (b) Cross-section of line marks under 3D microscope (color online)

As shown in Table 1, the bowing caused by the front finger grids had offsetting effect on the overall bowing of the cells. However, since the finger grids were slender and with only a tiny contact area, the offsetting effect was limited to 0.1 mm, as a result, the influence of the front finger grids on the bowing of the solar cells was ignored in this paper. The bowing of the cells which the laser-ablation direction was perpendicular to the trace direction was slightly larger than that of the parallel ones. However, the overlap area with the saw marks on the entire rear was negligible, which means it had nothing effect on the bowing after printing and firing, and the influence would be ignored in the subsequent analysis. Therefore, the influence of the front finger grids and the direction of laser-ablation can be ignored in the subsequent experiments. In the following parts, all conditions were ensured consistently with the saw marks in order to ensure accuracy in the subsequent experiments.

Table 1. Comparison of bowing by front fine Ag grid and the bowing in different laser-ablation direction

Laser-ablation ratio	Bowing/mm								Average/mm
2%(The front fine grid is printed)	2.1	2.1	2.2	2.0	2.1	2.2	2.1	2.2	2.13
2%(The front fine grid is not printed)	2.2	2.2	2.3	2.2	2.3	2.2	2.3	2.2	2.23
2%(perpendicular to the line mark)	2.2	2.2	2.2	2.2	2.2	2.1	2.3	2.2	2.20
2%(Parallel to line marks)	2.1	2.2	2.1	2.1	2.3	2.1	2.0	2.1	2.10

Based on previous discussion, we focused on the influence of different laser-ablation ratio to suppress the bowing effect. Laser-ablation ratio is the ratio of the laser-ablation area to the total area of the silicon wafer.

The Si wafers with the same conditions were divided into six groups with 5 pieces in each. Different laser-ablation ratio was respectively applied in laser-ablation. As shown in Table 2, the average bowing was 1.38 mm when the laser-ablation ratio was zero (that is, no laser-ablation), because the Al-Si alloy cannot be formed after SP without rear surface pattern. Though the bowing effect was suppressed at this condition, this treatment was meaningless because the whole rear surface was isolated. Meanwhile, the Al-Si contacts can only be generated in the laser-ablation area with the interaction of laser-ablation. Though excessive reduction of the laser-ablation area can reduce the bowing effect, the isolation of AlO_X/SiN_X will also significantly block the electrical performances of the cells. When the laser-ablation ratio increased from 0.05% to 8.00%, the bowing effect would gradually increase from 1.77 mm to 4.32 mm. One important reason is that different TCE of the Al layer and the Si layer at Al-Si contact areas, which cause the diverse shrinkage ability. When the firing temperature dropped below the Al-Si eutectic point (577 ℃), the bowing effect would be caused by the stress from the Al layer [27]. Hence, the Al-Si shrinkage area would be increased along with the enhanced stress of Al, leading to the bowing effect. However, the stress direction was always along the direction of laser-ablation. When the rear local contact was increased to a certain degree, the stress of aluminum rear-surface field (Al-BSF) would spread to all directions along the laser-ablation area. Then, higher ablation ratio can dramatically suppress the bowing effect. In Table 2, when the laser-ablation ratio reached 100%, the bowing effect was decreased to 3.06 mm. The increase of contact area would reduce the rear passivation area, which has an adverse effect on the rear surface recombination and reduced the minority carrier lifetime, but also reduced the long-wavelength response of the cells, since the rear passivation layer was also played as a back reflector. Thus it was undesirable to improve the bowing by increasing the laser-ablation ratio blindly. Similarly, the rear passivation layer was an insulating layer, which required laser-ablation to form current paths which Al-Si contacts can only be formed in the laser-ablation area. Therefore, reducing the laser-ablation area would also affect the electrical performances of the cell, which limited the decrease of the laser-ablation ratio.

Table 2. Comparison results of bowing corresponding to different laser-ablation ratio after printing and sintering

Laser-ablation ratio	Bowing /mm					Average /mm
0.00%	1.40	1.40	1.30	1.30	1.50	1.38
0.50%	1.70	1.80	1.80	1.75	1.80	1.77
2.12%	2.10	2.10	2.20	2.00	2.10	2.10
6.00%	2.90	2.80	2.80	2.85	2.85	2.84
4.00%	3.10	3.25	3.15	3.20	3.15	3.17
6.00%	3.70	3.65	3.70	3.65	3.60	3.66
8.00%	4.50	4.30	4.30	4.30	4.20	4.32
100.00%	3.00	3.20	3.00	3.10	3.00	3.06

Based on the experiments we have mentioned above, the Al-Si contact area had a strong impact on the bowing effect after printing and firing. Within a certain range, the bowing effect of the solar cells was on the rise with the increase of the laser-ablation ratio. Reasonable ablation ratio was essential for both passivation effect and electrical performance of solar cells. Then, the theoretical calculations and simulations were carried out to prove the accuracy of the experimental results.

The bowing effect of solar cells has been extensively investigated on temperature dependent firing and aluminum paste, investigations on patterns are rarely mentioned. Materials with different TCE can be modeled as a bimetallic strip (as shown in Fig. 2) [28]. The bowing stress was derived from temperature changes [29]. Hilali et al. (2007) modified the calculation equation of element bowing by considering the actual coverage area of Si and Al paste [26],

$$\delta = \frac{3(\alpha_{Al} - \alpha_{Si})(T_f - T_m)(t_{Al} + t_{Si})L^2}{4t_{Al}^2\left(4 + 6\frac{t_{Si}}{t_{Al}} + 4\left(\frac{t_{Si}}{t_{Al}}\right)^2 + \left(\frac{E_{Si}}{E_{Al}}\right)\left(\frac{t_{Si}}{t_{Al}}\right)^3 + \left(\frac{E_{Al}}{E_{Si}}\right)\left(\frac{t_{Al}}{t_{Si}}\right)\right)} \times S_f \quad (1)$$

where, t_{Si} was the thickness of the Si wafer, t_{Al} was the thickness of the Al paste, α_{Si} was the TCE of the Si wafer (3.36×10^{-6} K^{-1}), α_{Al} was the TCE of the Al paste (2.31×10^{-5} K^{-1}), T_f was the eutectic temperature (577 ℃), T_m was the measure temperature (room temperature 25 ℃), E_{Si} was the elastic modulus of the Si wafer (162.5 Gpa), E_{Al} was the elastic modulus of the Al paste (25.5 Gpa), L was the length of the solar cell, S_f was the laser-ablation ratio.

Poor electrical performances would be caused by the poor rear surface recombination and back electrodes if the Al-Si contact area was too large or too small. So this equation was only applicable to a certain range of contact

areas (1.00%-8.00%). It can be seen from the equation that keeping other conditions unchanged, in a certain range, the bowing gradually increased with the growing of the contact area.

For the calculation of the Al-Si contact area and the rear laser-ablation ratio S_f, the following model was applied, as shown in Fig. 4.

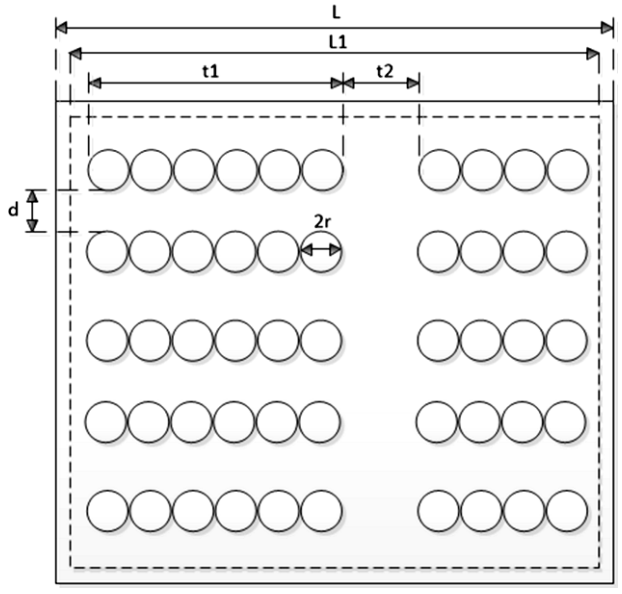

Fig. 4. Laser-ablation model on the rear surface of solar cells

We have carried out abundant experiments shown that the conversion efficiency of cells was appropriate with solid to dash lines combined laser-ablation pattern. Therefore, the pattern combining solid to dash lines was adopted in this experimental model. Here, t was the ratio of solid to dash lines, represented as $t = (t_1/(t_1+t_2))$ in Fig. 4. t_1 was the length of the laser action in the ratio of solid to dash lines, and t_2 was the distance between the laser actions in the ratio of solid to dash lines. m was the number of lines, d was the distance between lines, L^2 was the total area of the cell and L_1^2 was the entire area of the rear laser-ablation. Therefore, the laser-ablation ratio can be expressed by the following equation.

$$S_f = \frac{\pi r^2 m t L_1}{2L^2 r} \tag{2}$$

The number of laser-opening lines was determined by the laser-ablation area and spacing among the lines, and the solid to dash ratio was determined by the specific graphic design, so the laser-ablation ratio (S_f) can be expressed as follows,

$$S_f = \frac{\pi r L_1^2 t_1}{2L^2 d\left(t_1 + t_2\right)} \tag{3}$$

According to the bowing expression equation obtained from the model in Fig. 2, the bowing can be described as follows,

$$\delta = \frac{3\left(\alpha_{Al} - \alpha_{Si}\right)\left(T_f - T_m\right)\left(t_{Al} + t_{Si}\right)}{4t_{Al}^2\left(4 + 6\frac{t_{Si}}{t_{Al}} + 4\left(\frac{t_{Si}}{t_{Al}}\right)^2 + \left(\frac{E_{Si}}{E_{Al}}\right)\left(\frac{t_{Si}}{t_{Al}}\right)^3 + \left(\frac{E_{Al}}{E_{Si}}\right)\left(\frac{t_{Al}}{t_{Si}}\right)\right)} \times \frac{\pi r L_1^2 t_1}{2d\left(t_1 + t_2\right)} \tag{4}$$

As shown in Eq. (4), the bowing effect of the solar cells has a certain relationship with the thickness of the Si wafer, the thickness of the Al paste, the firing temperature, the ratio of the elastic modulus of the two layers, and the Al-Si contact area of the solar cells. It can be seen in the experiment, the bowing effect can be appropriately reduced by changing the contact area, which is in accordance with the description of Eq. (4).

The relationship between laser-ablation of laser area and the bowing effect can be clearly exhibited through the Abaqus finite element analysis (FEA) [30]. According to the profile of the firing temperature, stress was slightly induced when a liquid phase formed between the Al paste and the Si wafer. When the temperature was dropped below the Al-Si eutectic temperature (577 ℃), the material of the c-Si solar cells began to solidify and from ohmic contract. Therefore, an initial temperature of 577 ℃ was applied in the FEA model to analyze the bowing and residual stresses induced by collapsing temperature (from 577 ℃ to 25 ℃). Since the Al-Si contact only existed in the laser-ablation area, the two-layer model was only applied the Si-layer and Al-layer to neglect other influences. The material properties for numerical simulation are listed in Table 3 below,

Table 3. Material properties of Al paste and Si

Material	E (GPa)	γ	TCE (10^{-6} K^{-1})
Al paste	25.5	0.350	23.1
Si crystals	162.5	0.223	3.36

where, E was Young's modulus, γ was Poisson's ratio, TCE was the thermal coefficient expansion.

The model with the size of 158 mm × 9 mm was used in the FEA simulation to investigate the bowing changes, and the circular spot formed by the laser-ablation was approximately regarded as cubes of equal width. As shown in Fig. 5, t_1 is 700 μm and t_2 is 300 μm, the width of the small cuboid was the spot diameter. In addition, only the Si wafer and the Al paste were considered in the model calculations.

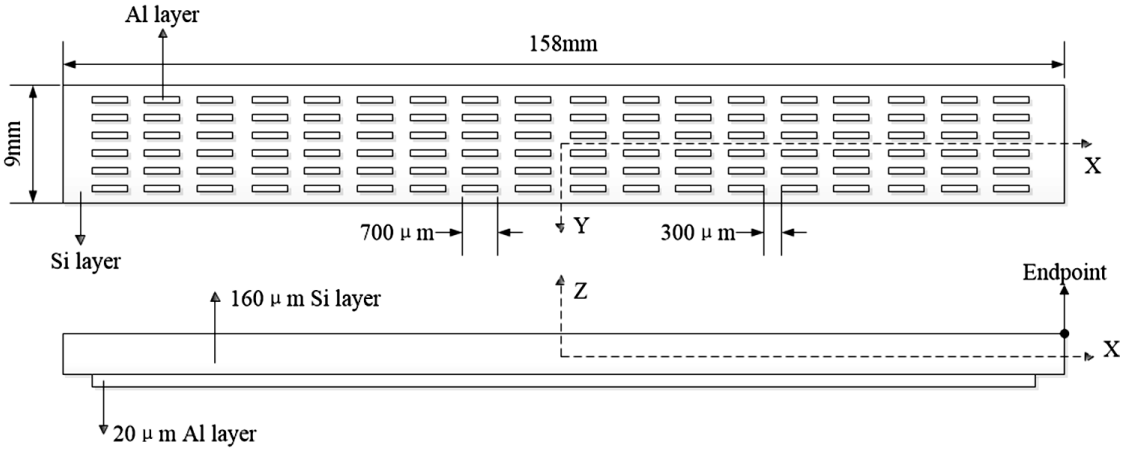

Fig. 5. Abaqus FEA simulation diagram

In the analysis of FEA, the center of the solar cell was defined as the coordinate origin. The model was divided into two parts: Al layer and Si bulk. The symmetric boundary conditions along the x-direction (U1=UR2=UR3=0) were set in the yz plane (x=0) and those along the y-direction (U2=UR1=UR3=0) were set in the xz plane (y=0), and one endpoint (Fig. 5) was completely fixed to avoid moving along other directions. The mesh used in the numerical simulation was a shell type defined as"C3D8 (8-node linear hexahedral element)" in Abaqus. The mesh should be divided to infinite small to obtain accurate simulation results. The FEA simulation results of the displacement and deformation in Si cell with the laser-ablation area of 2.11% after firing and cooling was exhibited in Fig. 6. The simulation result was in accordance with the actual experiments. The bowing data was obtained by observing the displacement of the z-axis U3 direction. Since the bowing was carried out in the negative direction of the Z axis, the maximum bowing amount in the negative direction was the maximum bowing deformation value of the Si cell. The bowing value of the silicon cell can be calibrated up to 1.484 mm through Fig. 6.

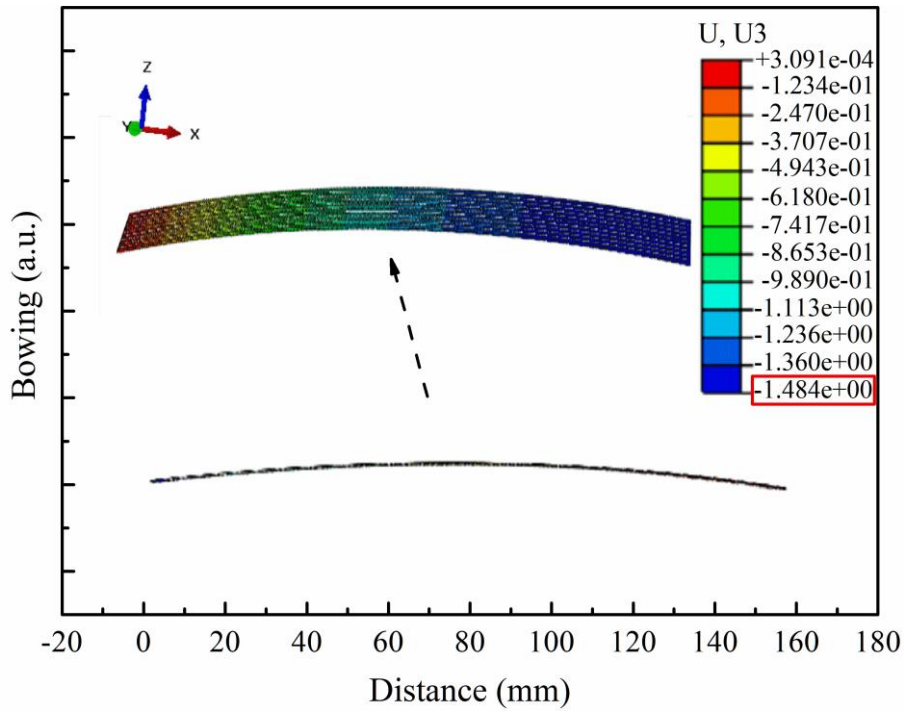

Fig. 6. The FEA simulation results of bowing effect in cell model when the laser-ablation area is 2.11% (color online)

However, the experiment results were poorly fitted to the calculation and simulation results as shown in Fig. 7. The results of calculation and simulation was dropped with the decreasing of the laser-ablation area, and finally closed to zero, while the experiment results were slightly higher. This is attributed to the mismatching between the Al layer and the Si layer in the simulation, where other factors such as the Ag paste, the existence of rear passivation layers and they were ignored. In general, the overall change tendency was roughly the identical, thus the influence trend of the Al-Si contact area on the bowing effect was obtained.

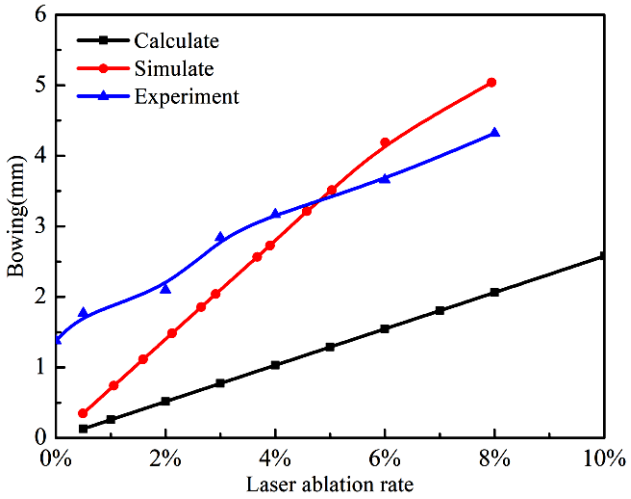

Fig. 7. Comparison of FEA simulation, calculation and experimental results (color online)

Narrow laser-ablation area can suppress bowing effect. The current extraction was required to ohmic contacts at interfaces through the insulated rear passivation layer. Therefore, excessively decreasing the laser-ablation area would drag the electrical performances down to a disaster. In the early stage of our studies, it was found that the conversion efficiency were relatively ideal determined when the laser-ablation ratio was 2.11%. Therefore, it should be considered that improving the bowing by changing different laser-ablation pattern with a constant laser-ablation area of 2.11%. It can be seen from Eq. (4) that in the design of the rear laser-ablation pattern, the bowing was related to the spot size, the thickness of the Si wafer and the ratio of solid to dash lines. The spot size of laser and thickness of Si were maintained at constant, indicating that the improvement of bowing effect can only be tuned by the ratio of solid to dash as shown in Fig. 8.

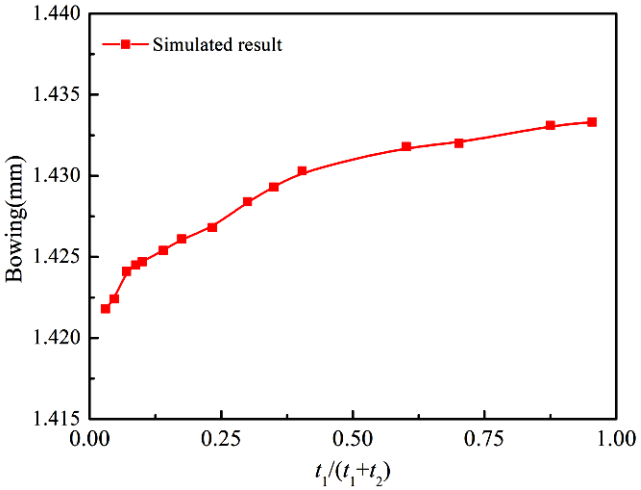

Fig. 8. The FEA simulation results of changing the solid to dash ratio (color online)

As shown in Fig. 8, the Al-Si contact area was kept unchanged at 2.11%, the bowing effect was decreased with the reducing of the ratio of solid to dash, and the laser-ablation pattern on the rear surface was gradually approaching a dot pattern. Therefore, the stress can be dispersed effectively by dispersing the light spot on the rear of the cells, thus improve the bowing. Based on this rule and combined with the conversion efficiency, a novel dotted pattern of laser-ablation was proposed in this paper. The light spot of the t_1 part was dispersed in the traditional back graphic, and adjusted the t_2 part at the same time. At this time, t_1 was close to the diameter of the spot (34 μm), and the solid to dash ratio ($t_1/(t_1+t_2)$) was 0.272. The bowing effect shown in Fig. 8 was 3.7% less than that of simulated backside design (1.484 mm) shown in Fig. 5. The decrease of bowing effect was owing to the release of stress with homogenous distributed Al-Si alloy. To verify the accuracy of the FEA simulation results of the novel dotted pattern, relevant experiments were sequentially carried to compare the two different pattern. The experiment was divided into two groups with 16 pieces in each with the laser-ablation area maintained constant at 2.11%. The experimental results were shown in Fig. 9.

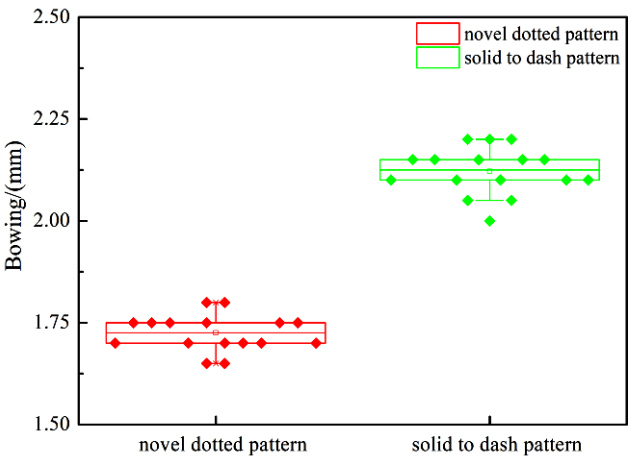

Fig. 9. Experimental results of different pattern (color online)

As shown in Fig. 9, the bowing effect was suppressed when the Al-Si contact pattern changed to the simulated results in FEA model. The average bowing effect of the novel dotted pattern was 0.397 mm lower than the conventional pattern, decreased to only 1.725 mm. The diameter of the laser spot used in this experiment was about 34 μm. The bowing effect was most optimized after applying the novel designed laser-ablation pattern.

4. Conclusions

The bowing effect caused by the difference in TCE of the Al layer and the Si layer hinders the development of high-efficiency thin-film cells. The work in this paper has fully investigated the influence of the Al-Si contact area on the bowing of the MWT+PERC high efficiency cells from the point of laser process on the rear surface. Both simulations and experiments were indicated that the bowing effect was decreased with the reducing of the Al-Si contact area. Combined with the conversion efficiency, the laser-ablation ratio was kept unchanged at 2.11%. A novel dotted pattern of laser-ablation was proposed in this article through tuning the ratio of solid to dash. In this scheme, the ratio of solid to dash (*t*) was 0.272 and the light spots on the rear surface was dispersed. Under the same laser-ablation area, this design can improve bowing effect due to release of stress in Al-Si alloy. This design was confirmed by both simulation and experiment, which has provided prospects for subsequent improvement of bowing effect.

Acknowledgement

This research was supported by "National Natural Science Foundation of China (Grant No. 61804066)" & "Natural Science Foundation of Jiangsu Province (Grants No. BK20180596, BK20180601)" & "China Postdoctoral Science Foundation (2020M671602)" & "Jiangsu Postdoctoral Science Foundation (2020K143B)" & "Postgraduate Research & Practice Innovation Program of Jiangsu Province (Grants No. KYCX19_1858)".

References

[1] D. Suh, Thin Solid Films **668**, 45 (2018).
[2] M. Görig, C. Breyer, Environ. Prog. Sustain. Energy **35**(3), 914 (2016).
[3] A. Schneider, C. Gerhards, P. Fath, E Bucher, R. J. Young, J. A. Raby, A. F. Carroll, Conference Record of the 29th IEEE Photovoltaic Specialists Conference **2002**, 336 (2002).
[4] S. Kim, S. Sridharan, C. Khadilkar, A. Shaikh, Conference Record of the 31st IEEE Photovoltaic Specialists Conference **2005**, 1100 (2005).
[5] V. Pogue, S. N. Melkote, S. Danyluk, Mat. Sci. Semicon. Proc. **75**, 173 (2018).
[6] M. Köntges, I. Kunze, S. Kajari-Schröder, X. Breitenmoser, B. Bjorneklett, Sol. Energy. Mat. Sol. Cells **95**, 1131 (2011).
[7] P. Yoon, H. Chung, H.-E. Song, J. H. Seo, S. Shin, Appl. Therm. Eng. **90**, 559 (2015).
[8] L. Janßen, M. Rinio, D. Borchert, H. Windgassen, D. L. Bätzner, H. Kurz, Res. Appl. **15**(6), 469 (2007).
[9] F. Huster, Conference Record of 20th European Photovoltaic Solar Energy Conference and Exhibition Barcelona **2005,** 635 (2005).
[10] J. Lim, S. Kim, H.-K. Ahn, H.-E. Song, G. Kang, Energies **12**, 1593 (2019).
[11] C. Mader, U. Eitner, S. Kajari-Schröder, R. Brendel, IEEE J. Photovolt. **3**, 2156 (2012).
[12] Y. Okada, Y. Tokumaru, J. Appl. Phys. **56**, 314 (1984).
[13] F. Nix, D. MacNair, Phys. Review - Phys. Rev. X **60**, 597 (1942).
[14] C.-M. Lai, C.-H. Su, K.-M. Lin, Appl. Therm. Eng. **55**, 7 (2013).
[15] J. Murray, A. McAlister, Bull. Alloy Phase Diagrams **5**, 74 (1984).
[16] M. Demant, S. Rein, J. Krisch, S. Schoenfelder, C. Klute, S. Bartsch, R. Preu, Proceedings of the IEEE Photovolt. Specialists Conference (PVSC), pp. 001641 (2011).
[17] C. Tool, A. Burgers, P. Manshanden, A. W. Weeber, Conference Record of 17th European Photovoltaic Solar Energy Conference **2001**, 40 (2001).
[18] S. Pingel, Y. Zemen, O. Frank, T. Geipel, J. Berghold, in Proceedings of the 24th European Photovoltaic Energy Conference (2009).
[19] C. Kohn, T. Faber, R. Kübler, J. Beinert, G. Kleer, F. Clement, D. Erath, I. Reis, F. Martin, A. Müller, Fraunhofer ISE 1270 (2020).
[20] X. Gu, X. Yu, J. Xu, R. Fan, D. Yang, Progress in Photovol.: Res. Appl. **21**, 456 (2011).
[21] F. Clement, M. Menkoe, D. Erath, T. Kubera, R. Hoenig, W. Kwapil, W. Wolke, D. Biro, R. Preu, Sol. Energy. Mat. Sol. Cells **94**(1), 51 (2010).
[22] H. Knauss, M. McCann, P. Fath, Conference Record of the 31st IEEE Photovoltaic Specialists Conference **2005,** 1201 (2005).
[23] F. Clement, M. Menkoe, T. Kubera, C. Harmel, R. Hoenig, W. Wolke, H. Wirth, D. Biro, R. Preu, Sol. Energy. Mat. Sol. Cells **93**(6), 1051 (2009).
[24] M. Nicolai, M. Zanuccoli, P. Magnone, D. Tonini, E. Sangiorgi, C. Fiegna, J. Comput. Electron. **15**(1), 277 (2016).
[25] M. Hendrichs, B. Thaidigsmann, E. Lohmüller, S. Nold, F. Clement, D. Biro, B. Rech, R. Preu, Energy Technology **2**(1), 34 (2014).
[26] M. Hilali, J. M. Gee, P. Hacke, Sol. Energy. Mat. Sol. Cells **91**(13), 1228 (2007).
[27] O. Kraft, W. D. Nix, J. Appl. Phys. **83**, 3035 (1998).
[28] C.-H. Chen, H.-T. Hu, F.-M. Lin, H.-H. Hsieh, J. Zhejiang Univ.-Sc. A **18**(1), 49 (2017).
[29] V. A. Popovich, M. Janssen, I. M. Richardson, T. van Amstel, I. J. Bennett, Sol. Energy. Mat. Sol. Cells **95**(1), 93 (2011).
[30] P. Yoon, T. Baek, H. Chung, H.-E. Song, S. Shin, Solar Energy **105**, 705 (2014).

*Corresponding author: xi.xi@jiangnan.edu.cn